**MINI-REVIEW**

# Aerosolised micro and nanoparticle: formulation and delivery method for lung imaging

Miftakul Munir[1] · Herlan Setiawan[1] · Rohadi Awaludin[1] · Vicky L. Kett[2]

## Abstract

**Purpose** The application of contrast and tracing agents is essential for lung imaging, as indicated by the wide use in recent decades and the discovery of various new contrast and tracing agents. Different aerosol production and pulmonary administration methods have been developed to improve lung imaging quality. This review details and discusses the ideal characteristics of aerosol administered via pulmonary delivery for lung imaging and the methods for the production and pulmonary administration of dry or liquid aerosol.

**Methods** We explored several databases, including PubMed, Scopus, and Google Scholar, while preparing this review to discover and obtain the abstracts, reports, review articles, and research papers related to aerosol delivery for lung imaging and the formulation and pulmonary delivery method of dry and liquid aerosol. The search terms used were "dry aerosol delivery", "liquid aerosol delivery", "MRI for lung imaging", "CT scan for lung imaging", "SPECT for lung imaging", "PET for lung imaging", "magnetic particle imaging", "dry powder inhalation", "nebuliser", and "pressurised metered-dose inhaler".

**Results** Through the literature review, we found that the critical considerations in aerosol delivery for lung imaging are appropriate lung deposition of inhaled aerosol and avoiding toxicity. The important tracing agent was also found to be Technetium-99m ($^{99m}$Tc), Gallium-68 ($^{68}$Ga) and superparamagnetic iron oxide nanoparticle (SPION), while the essential contrast agents are gold, iodine, silver gadolinium, iron and manganese-based particles. The pulmonary delivery of such tracing and contrast agents can be performed using dry formulation (graphite ablation, spark ignition and spray dried powder) and liquid aerosol (nebulisation, pressurised metered-dose inhalation and air spray).
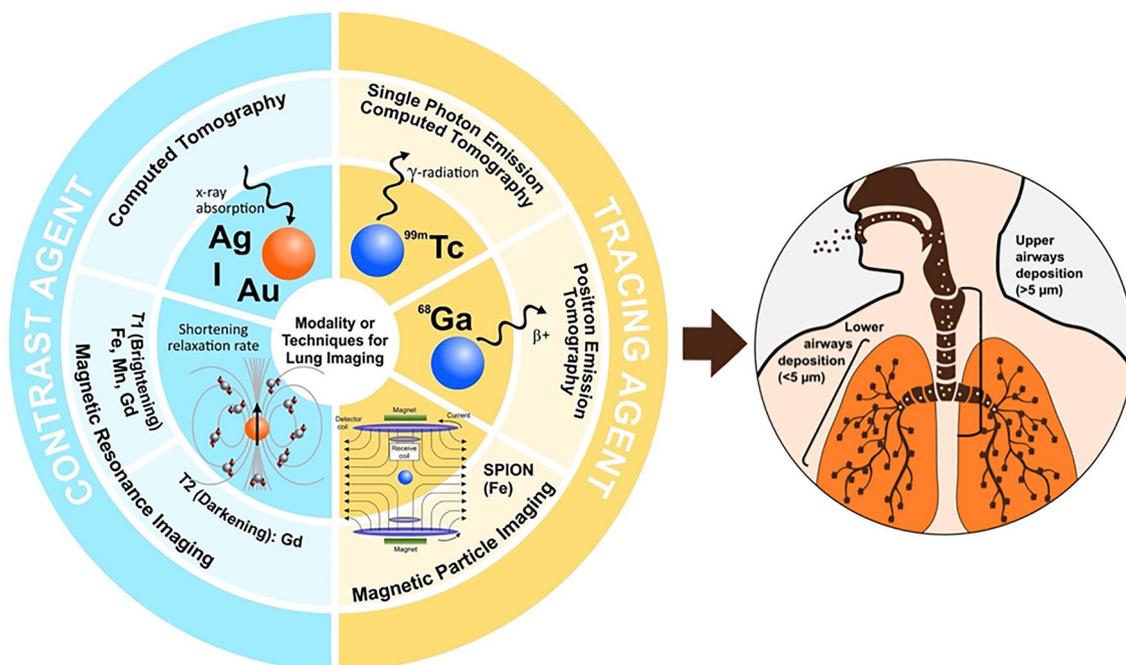
**Conclusion** A dual-imaging modality with the combination of different tracing or contrast agents is a future development of aerosolised micro and nanoparticles for lung imaging to improve diagnosis success.

✉ Miftakul Munir
    mift008@brin.go.id

1   Research Center for Radioisotope Radiopharmaceutical
    and Biodosimetry Technology, National Research
    and Innovation Agency, South Tangerang 15345, Indonesia

2   School of Pharmacy, Queen's University Belfast, 97 Lisburn
    Road, Belfast BT9 7BL, UK

**Graphical abstract**

## Abbreviations

| | |
|---|---|
| Ag | Silver |
| AgNP | Silver-based nanoparticle |
| Au | Gold |
| AuNP | Gold-based nanoparticle |
| CA | Contrast agent |
| CHF | Chronic heart failure |
| COPD | Chronic obstructive pulmonary disease |
| COVID-19 | Coronavirus disease 2019 |
| CT | Computed tomography |
| DOTA | Dodecane tetraacetic acid |
| DTPA | Diethylenetriamine pentaacetic acid |
| EANM | European Association of Nuclear Medicine |
| FeNP | Iron-based nanoparticle |
| FPF | Fine particle fraction |
| $^{68}$Ga | Gallium-68 |
| Gd | Gadolinium |
| HU | Hounsfield units |
| I-CA | Iodonated-based contrast agent |
| MDP | Methylene diphosphonate |
| MnNP | Manganese nanoparticle |
| MPI | Magnetic particle imaging |
| MRI | Magnetic resonance imaging |
| MRP1 | Multidrug resistance protein-1 |
| NIV | Non-invasive ventilation |
| OB | Olfactory bulb |
| PE | Pulmonary embolism |
| PEG | Polyethylene glycol |
| PET | Positron emission tomography |
| pMDI | Pressurised metered-dose inhaler |
| PVA | Polyvinyl alcohol |
| SASD | Supercritical $CO_2$-assisted spray drying |
| SPECT | Single-photon emission computed tomography |
| SPIONs | Super paramagnetic iron oxide nanoparticles |
| T1 | Longitudinal |
| T2 | Transverse |
| $^{99m}$Tc | Technetium-99m |
| TEM | Transmission electron microscopy |
| WHO | World Health Organization |

## Introduction

Lung disease is one of the major causes of illness-related death, accounting for approximately six million deaths worldwide in 2019 (12% of total deaths) [1]. This number can remain unchanged in the future, as predicted by The Global Burden of Disease study, in which chronic obstructive pulmonary disease (COPD) and lower respiratory infection will be the third and fourth cause of death globally in 2030, respectively [2]. Furthermore, lower respiratory

infection is predicted to rise in the future, particularly in tropical countries, due to the increased infectious activity of non-tuberculous mycobacteria, which tends to infect people with either genetic or acquired structural typical lung diseases, such as COPD and cystic fibrosis [3]. This condition is worsened by the emergence of coronavirus disease 2019 (COVID-19), which has become a global pandemic and has caused more than 6.24 million deaths around the world, as reported by the World Health Organization (WHO) [4]. Aside from the high mortality rate, lung disease is also predicted to be one of the global burdens of severe health-related suffering until 2060 [5]

The economic burden is one of the global impacts of lung diseases, caused by either unnecessary drug overprescription or treatment failure due to over-or underdiagnosis, respectively [6]. For example, studies on COPD misdiagnosis revealed that the underdiagnosis and overdiagnosis prevalence of this disease was 56.7–81.4% and 29.0–65.0%, respectively [7], leading to 55.4% dissipation of treatment cost [8]. The misdiagnosis of lung disease not only aggravates the economic burden but also can increase mortality due to false medical treatment. For instance, lung cancer is frequently misdiagnosed as tuberculosis in a country with tuberculosis prevalence. This phenomenon highlights the importance of lung diagnosis to reduce the lung disease burden and its mortality rate [9].

Lung imaging, comprising of computed tomography (CT), magnetic resonance imaging (MRI), positron emission tomography (PET), and single-photon emission computed tomography (SPECT), is a standard method in lung disease diagnosis, as presented in Table 1. Nevertheless, each modality for lung imaging has weaknesses, such as the limited spatial resolution in molecular imaging-based modality [10–12]. To increase the performance of such a diagnosis method, micro and nano-inhalable particles have been investigated and applied for decades as a tracing agent or contrast agent [13–15]. As a tracing agent, the lung deposition of an inhaled particle can be detected due to the nature of the particle; for example, Technetium-99m ($^{99m}$Tc) emits gamma-ray, which can be detected by SPECT, resulting in an image of the lung [13]. On the other side, the contrast agent can alter the result of existing imaging methods (CT and MRI), providing brighter or darker regions for better diagnosis or interpretation [16–18].

To date, 38 tracing and contrast agents have been approved for commercial use [30–32], and the development of new agents is underway to improve the safety aspect and image quality [17, 18, 23, 33, 34]. This review aimed to

**Table 1** Detection mechanism in lung imaging

| Detection source | | Imaging method | Advantages | Disadvantages |
|---|---|---|---|---|
| Element | Mechanism | | | |
| *Tracing agent* | | | | |
| $^{99m}$Tc | Gamma energy (140 keV) | SPECT | Trace amount is required (nanomolar) [19] | Radiations, limited spatial resolution (~ 15 mm), no lung morphology image [12] |
| $^{68}$Ga | Positron ($E_{max} = 1899$ keV) | PET | Trace amount is required (nanomolar) [19] | Radiations, limited spatial resolution (~ 6 mm), no lung morphology image [12] |
| AuNP | X-ray absorption | CT | Therapeutic effect (photothermal and radiosensitiser) [20, 21] | higher concentration required compared to other CAs [22] |
| AgNP | X-ray absorption | CT | Antimicrobial activity [23] | Easy to be deposited in other tissues after pulmonary delivery [24] |
| *Contrast agent* | | | | |
| FeNP | Shortening the T1 relaxation time of nearby water | MRI | Magnetic hyperthermia therapy [25] | Inflammatory response and extrapulmonary toxicity were observed upon inhalation [26] |
| | Imaging electronic magnetisation of SPIONs | MPI | | |
| GdNP | Shortening the T1 and T2 relaxation time of nearby water | MRI | Radiosensitiser [27] | Toxicity of free ion [14] |
| MnNP | Shortening the T1 relaxation time of nearby water | MRI | Enhancement of photo- and chemo-therapy [28] | Neurotoxicity upon inhalation [29] |
| I-CA | X-ray absorption | CT | Low cost [30] | IODINE sensitivity and high osmolality [30] |

AgNP, silver-based nanoparticle; AuNP, gold-based nanoparticle; CA, contrast agent; CT, computed Tomography; FeNP, iron-based nanoparticle; $^{68}$Ga, Gallium-68; I-CA, iodonated-based contrast agent; MnNP, manganese nanoparticle; MRI, magnetic resonance imaging; PET, positron emission tomography; SPECT, Single photon emission computed tomography; SPIONs, super paramagnetic iron oxide nanoparticles; T1, longitudinal; T2, transverse; $^{99m}$Tc, Technetium-99m

address the challenges of pulmonary delivery for lung imaging, as well as the aerosol formulations that have been commercially approved or are still in development study. There have been reviews on the application of nano or microparticles for imaging diagnosis purposes (CT: [15, 22]; MRI: [14, 35, 36]; PET: [37]; SPECT: [38, 39]), but there is no review which discusses the application of aerosol for lung imaging. This review is focused on understanding the critical parameters of aerosol delivery into the lung, which are essential for formulating micro- or nanoparticles for pulmonary delivery. Furthermore, the fundamental concepts of different aerosol production methods that contribute to the development of aerosolised contrast and tracing agent for lung imaging quality improvement are also discussed. We explored several databases, including PubMed, Scopus, and Google Scholar, during preparing this review to discover and obtain the abstracts, reports, review articles, and research papers related to aerosol delivery for lung imaging and the formulation and pulmonary delivery method of dry or liquid aerosol. The following search terms were used: "dry aerosol delivery", "liquid aerosol delivery", "MRI for lung imaging", "CT scan for lung imaging", "SPECT for lung imaging", "PET for lung imaging", "magnetic particle imaging", "dry powder inhalation", "nebuliser", and "pressurised metered-dose inhaler".

## Challenges of aerosol delivery for lung imaging

Pulmonary delivery for contrast or tracing agent administration route has provided an image for lung disease diagnosis for decades [13]. Furthermore, an attempt to discover new inhalable particles with increased image quality and safety profile has also been reported in recent years [17, 18, 23, 33, 34]. For instance, Silva et al. reported the development of a dual-modality contrast agent consisting of Fe and gold (Au) for detection using MRI and CT, respectively [20]. Despite its success in lung imaging and potential for future development, several challenges need to be overcome in designing inhalable particles for tracing or contrast agents.

## Toxicity

The first challenge is attributed to the toxic nature of different tracing and contrast agents. The established tracing agents are typically an element with radioactive hazards due to ionising radiation or particle emission. Nevertheless, typical radionuclides used for diagnosis are considered safe due to the low radiation energy and short half-life [13]. $^{99m}$Tc, Tc, is the most widely used diagnostic radionuclide, including in lung scintigraphy. It has a half-life of 6 h and a gamma energy of 140 keV, yet sufficient for diagnosis purposes. [40]. Another radionuclide used for lung scintigraphy, Gallium-68 ($^{68}$Ga, a positron-emitting radionuclide), has a shorter half-life (67.71 min) with $E_{max}$ of 1899 keV [41]. The amount of radioactive element used for the diagnostic purpose is also meagre; for instance, the typical radioactivity of $^{99m}$Tc for clinical use is 185–925 MBq, equal to only 0.95–4.70 ng of Tc metal [19]. On the other hand, a significantly higher amount of element is required for the contrast agent, leading to potential toxicity in the human body. Another issue in the use of radioactive tracing agents is the possibility of free radionuclide release from radiolabelled compound or complex, leading to free radionuclide extrapulmonary distribution. For instance, free pertechnetate has been found in thyroid upon lung scintigraphy due to unstable radiolabelled compound or complex [42]. Although such extrapulmonary distribution will not harm the organs, free radionuclides in significant amounts can disturb lung scintigraphy [43, 44]. Therefore, standard quality control for radiopharmaceuticals, e.g., radiochemical purity, should also be performed in the lung scintigraphy.

As an endogenous element in the human body, the use of iron (Fe) as a contrast agent is considered safe since ionic Fe presents as a complex with binding protein and the metal one has a low bio-solubility. Different binding and regulatory proteins are available for Fe absorption in the human digestive system without toxic effects [45]. However, such absorption facilitation is significantly limited in the respiratory tract, which might induce local adverse effects, such as inflammatory response. Furthermore, the inhaled Fe can easily be transported to other organs and causes more severe effects, including pro-atherosclerotic effect and alteration of autonomic regulation [26]. Similar to Fe, the inhalation of different elements for contrast agents can potentially induce intra- or extrapulmonary side effects, where the result can be even worse for exogenous substances, i.e. Au [46], gadolinium (Gd), and silver (Ag) [47]. In general, although the toxicity of these elements is enhanced in the ionic form [32], the nanoparticle form can also induce cell death due to the easy cellular uptake, resulting in cellular toxicity [26]. The toxicity of the iodinated contrast agent relies on the molecular form, in which inorganic iodine and ionic compounds exhibit higher toxicity [30].

Continuous efforts have been made toward minimising the toxicity of contrast agents, including the formulation of the stable complex to avoid the release of free ionic elements and interaction with cellular membranes, proteins, and other biological structures [30, 48]. Another attempt to reduce the toxicity is minimising cellular uptake, and particle absorption into the systemic circulation, which can be achieved by preparing micron or sub-micron size particle since effective cellular membrane penetration can only effectively occurs in size of < 200 nm [49]. Although larger particles can still be engulfed by alveolar macrophage, this type of cell is able to generate protein complex to minimise the toxicity of quantitatively large metallic element absorption, such as Fe [50].

## Radio-protection of radioactive aerosol or gas

Radioactive contamination is one of the concerns during the utilisation of radiopharmaceuticals in the medical field. Common liquid radiopharmaceuticals typically pose a low contamination risk, requiring simple handling during preparation and administration to the patients. On the other hand, radioactive aerosol poses a relatively higher risk due to its nature that easily diffuses into the air. Brudecki et al. reported that the activity of $^{99m}$Tc aerosol in a typical ventilation-perfusion SPECT facility ranged from $99 \pm 11$ to $6.1 \pm 0.5$ kBq m$^{-3}$, resulting in daily intake by male technicians, female technicians, male nurses and female nurses of 5.4 kBq, 4.4 kBq, 3.0 kBq and 2.5 kBq, respectively [51]. Although such internal contaminations are considered safe for the medical staff (over three orders of magnitude lower than the dose limit), the contamination level should be kept as low as possible to avoid the reduction of gamma camera performance [52].

## Lung deposition

Aside from toxicity and radio-protection concern, designing the inhalable particle size should also consider lung deposition since particle larger than 5 μm is most likely deposited in upper airways, followed by rapid pulmonary clearance and resulting in poor lung image in the healthy lung [39]. The presence of disease in the lung is most likely to alter the particle deposition due to the decrease in airway cross-section. Several studies, as presented in Table 2, revealed that most lung diseases enhanced lung deposition, although the deposition pattern has become more heterogenous as some areas are poorly ventilated and less penetrated by inhaled particles [53]. Such a condition will lead to great disadvantages in lung disease therapy since the drug bioavailability will be under or over the therapeutic window in some areas, resulting in underdose or toxic effects, respectively [54, 55]. For diagnostic purposes, the heterogenous deposition of inhaled particles might not be disadvantageous since less penetrated lung area can be an indication of a certain disease. Nevertheless, a particular aerodynamic size range is still required to ensure that the lung deposition is adequate for generating a good diagnostic image [53].

As seen in Table 2, the lung deposition of inhaled particles with an aerodynamic size of 1–5 μm was typically not affected or increased in the presence of lung diseases. Brown et al. suggested that although obstructed airways in diseased lungs should have reduced lung deposition, mucociliary clearance impairment and slow-deep breathing patterns can enhance the deposited particles and make them similar to those of the healthy lung [56]. Higher particle deposition in the diseased lung is also possible, as reported by Furi et al., since narrower airways induce airflow turbulence

resulting in higher inertial impaction. Such a higher deposition might also be induced by the use of polydisperse particles (82–5960 nm), where larger particles will be retained in the upper airways, while smaller ones penetrate deeper lung [57]. In contrast, monodisperse particles are most likely to give more heterogenous lung deposition since large particles will only be deposited in the upper area, and ultrafine particles tend to be exhaled [58–60]. To ensure the size of inhalable particles falls within the desirable range, especially for underdeveloped products, in vitro aerosolisation devices, e.g., cascade impactor, can be utilised for quality control [54].

It can be concluded that the inhalable powder should be designed in a size of 200 nm–5 μm to minimise systemic absorption and to reach deep lung deposition for the best quality image and to minimise systemic absorption, respectively, although the presence of a particular disease inducing airways obstruction requires smaller inhaled particles to reach deep lung effectively. Different formulations and aerosol delivery methods have been developed to achieve this purpose, as discussed in the next section (Fig. 1).

## Formulation and aerosol delivery method into respiratory airways

### Dry aerosol

Dry formulation provides a stable form, which can be stored for a long time. However, the main challenge of this form is the preparation method, which might require a sophisticated instrument to produce an ideal dry aerosol for pulmonary delivery [54].

### Graphite ablation

Graphite ablation method is used in Technegas to produce $^{99m}$Tc-radiolabelled carbon aerosol with a size of < 100 nm for lung ventilation scintigraphy [70]. $^{99m}$Tc-pertechnetate in saline solution yielded from $^{99}$Mo/$^{99m}$Tc generator is used as $^{99m}$Tc source in this method. The $^{99m}$Tc-radiolabelled carbon aerosol generation method has been detailed in a review by Wiebe et al. as illustrated in Fig. 2 [71]. In brief, $^{99m}$Tc solution is added to a crucible, followed by evaporation at 70ºC for 6 min in an ultrapure argon environment. Subsequently, graphite and $^{99m}$Tc are ablated by an alternating-current arc generated between the terminals holding the crucible. Aerosolised carbon nanoparticles are produced by heating at 2750 °C for 15 s in an ultrapure argon environment [13].

Carbon nanoparticle generated from the graphite ablation method has a size of < 140 nm with a gas-like characteristic upon aerosolisation, which provides an ideal lung deposition for imaging purpose [13, 71]. Many studies reported different sizes of carbon aerosol from Technegas,

**Table 2** The inhaled particle deposition in different clinical lung conditions

| Clinical indication | Inhaled particles | Aerodynamic size | Key findings | References |
|---|---|---|---|---|
| (AAT) deficiency | [99mTc]-AAT (nebulisation into human airways) | 4 μm | No significant difference in lung deposition in the healthy and diseased lung (C/P ratio 1.48–1.66) | [61] |
| CF | [99mTc]-AAT (nebulisation into human airways) | 4 μm | No significant difference in lung deposition between the healthy and diseased lung (C/P ratio 1.37–1.48) | [61] |
| | [99mTc]-iron oxide (nebulisation into human airways) | 4.6–4.9 μm | No significant difference in lung deposition between the healthy and diseased lung (C/P ratio 1.02–1.78) | [56] |
| | Levofloxacin (nebulisation into lung model) | 3.65 μm | Lung deposition in CF was higher (30–50%) than in healthy lung (15–30%) | [62] |
| | [99mTc]-DTPA-Tobramycin (nebulisation into human airways) | eFlow: 3.95 μm | Lung deposition in CF was lower (26.6%) than in healthy lung (40.0%) | [63] |
| | | LC: 3.54 μm | No significant difference in lung deposition between the healthy and diseased lung (44.3–45.2%) | |
| COPD | Diesel exhaust particle | 10–500 nm | The deposition fraction increased with increasing the severity of the disease. The deposition fraction of particles of < 100 nm was decreased in COPD patients | [58] |
| | Polystyrene latex nanospheres (Electrospray aerosol generation into human airways) | 50 and 100 nm | The deposition fraction was significantly lower in the lung with emphysema compared to healthy ones ($p = 0.001$–0.01) | [64] |
| | Polystyrene latex nanospheres (Electrospray aerosol generation into human airways) | 50 nm | Exhaled particle in COPD was significantly higher (0.128) compared to the healthy one (0.074) ($p = 0.01$) | [59] |
| | [99mTc]-carbon/Technegas (aerosolisation into human airways) | 100 nm | No significant difference in lung deposition, retention, and clearance in COPD and healthy lung | [65] |
| | Particulate matter in the air of industrial area | 82–5960 nm | Lung deposition was significantly higher in the diseased lung compared to healthy ones | [57] |
| Asthma | Nanocarbon (spark generator) | 23 nm | The efficient respiratory deposition was higher in subjects with asthma | [66] |
| | Aerosolisation into lung model | man: 8.1 μm chi: 6.1 μm | The deposition is significantly higher in the upper airways of the asthmatic model compared to healthy ones | [67] |
| | [99mTc]-BDP/FF combination (nebulisation into human airways) | BDP: 1.5 μm FF: 1.4 μm | No significant difference in lung deposition in the healthy and diseased lung (54.9–56.2%) | [68] |
| OLD, RLD | DEHS (aerosolised into human airways) | 0.02–0.24 μm | Lung deposition was increased in OLD and unchanged in RLD compared to healthy ones | [69] |

AAT, a1-antitrypsin; CF, cystic fibrosis; COPD, chronic obstructive pulmonary disease; DEHS, di-2-ethylhexyl sebacate; C/P ratio, central to peripheral ratio; OLD, obstructive lung disease; RLD, restrictive lung disease

depending on the particle collection and characterisation methods [72]. For instance, the use of electrostatic precipitation and transmission electron microscopy (TEM) by Senden et al. reported size of 30–60 nm, while a 400-mesh filter coupled with glass-fibre filter paper and photo correlation spectroscopy resulted in a size of 97–140 nm [71, 73]. A size of ~ 100 nm observed from Technegas is most likely due to the aggregation upon particle collection [71].

As an inhalable particle, carbon aerosol with a size of < 140 nm will follow Brownian diffusion upon inhalation, leading to deposition in the alveolar region and lower respiratory tracts [54]. Such lung deposition is considered
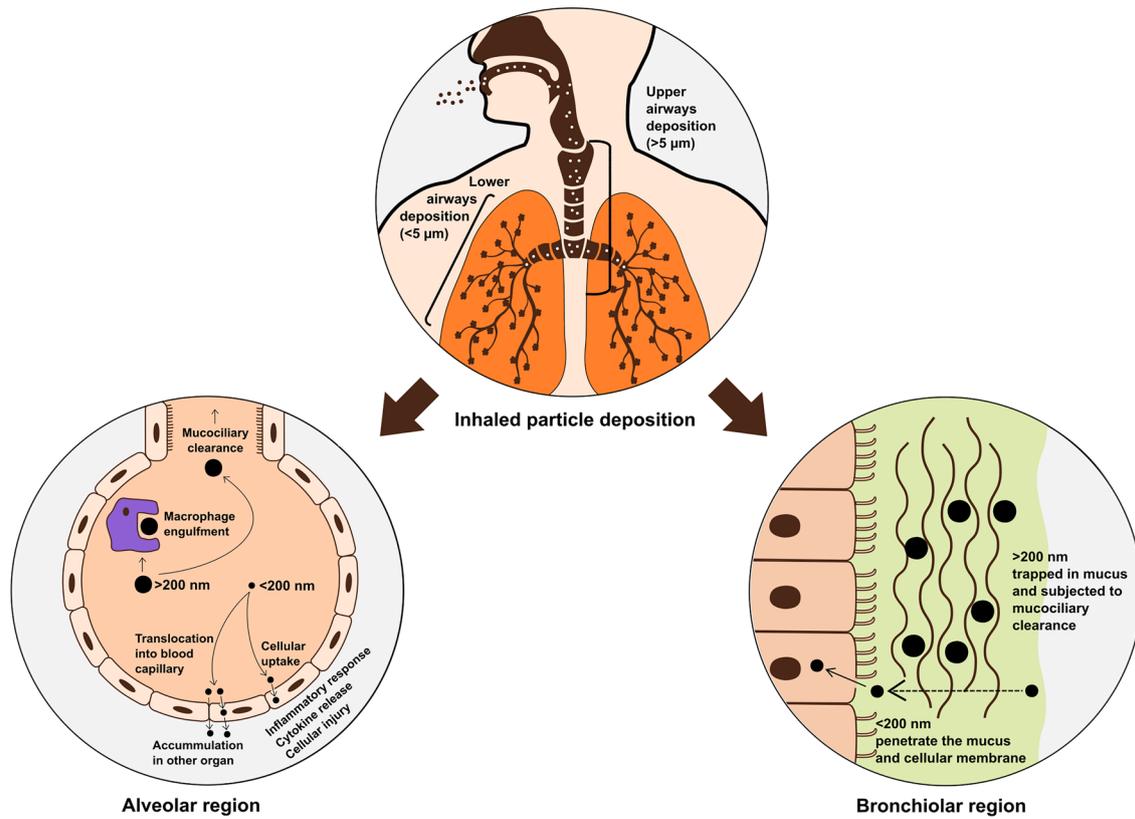
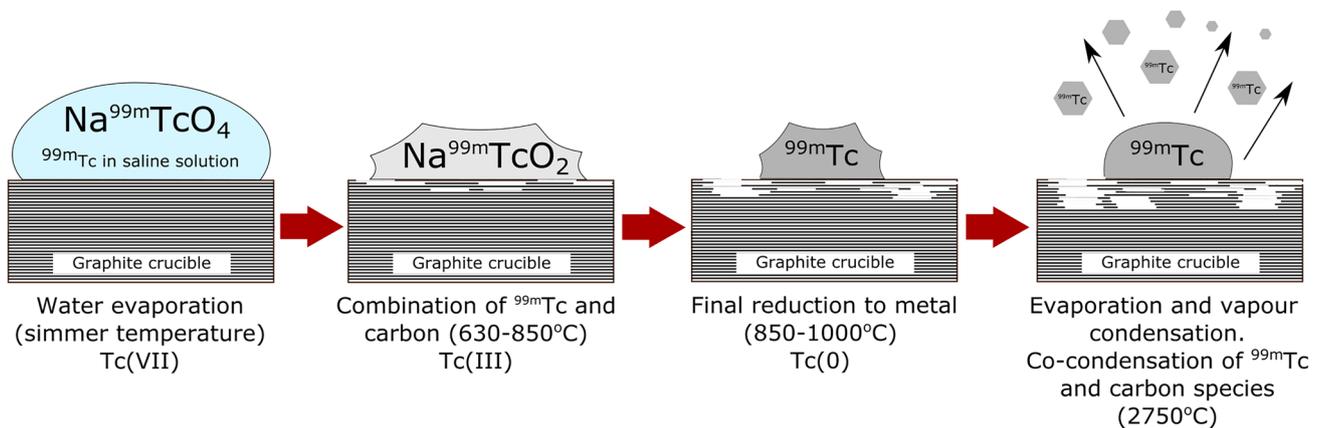**Fig. 1** The fate of inhaled particles depends on their size [26, 54]



**Fig. 2** Production of $^{99m}$Tc-carbon aerosol by graphite ablation method. Adapted from Wiebe et al. [71]

an ideal particle distribution for lung imaging [74]. Such particle size for inhalable particles theoretically can easily penetrate the cellular membrane and induce toxicity [49]. Nevertheless, the clinical use of Technegas for more than three decades proves the safety of the $^{99m}$Tc-labelled carbon aerosol [13, 71]. This safety profile can be explained by the

fact that the amount of carbon nanoparticles inhaled is very low, which means the toxicity effect can be neglected [75]. Furthermore, a study by Zhang et al. revealed that carbon nanoparticles with a size of < 100 nm showed no toxicity in RAWS264.7 cells, and a toxic effect was observed in the nanoparticle in size of > 250 nm [76]. A review by Pacurari

et al. also demonstrated that multi-walled carbon nanotubes with smaller sizes were less potent in inducing lung fibrosis upon inhalation [77].

Due to an ideal lung distribution and no toxicity, $^{99m}$Tc-labelled carbon aerosol has been widely used in lung imaging to diagnose different lung-related diseases, such as COPD, pulmonary embolism (PE), and tracheobronchitis [38, 78, 79]. Nasr et al. reported that lung scintigraphy by $^{99m}$Tc-labelled carbon aerosol in COVID-19 patients has successfully diagnosed COPD and PE [74]. The same method has also found the presence of tracheobronchitis in COVID-19 patients by observing an increase in tracheobronchial uptake of $^{99m}$Tc-labelled carbon aerosol, as reported by Verger et al. [70]. In conclusion, graphite ablation method generates radiolabelled carbon aerosol ideal for lung ventilation scintigraphy. Nevertheless, graphite ablation is a sophisticated method and can only be performed using a commercial aerosol generator called Technegas.

### Spark ignition

Spark ignition method has been utilised to produce different nanoparticles, including alloy, composite, metal, oxide, and semiconductor [80]. This method generates nanoparticles as an aerosol via spark discharge from two heated conducting electrodes with gas flow, as illustrated in Fig. 3 [81]. Similar to graphite ablation, this method spontaneously produces nanoparticles directly from large and solid material, resulting in spherical particle with a size of < 10 nm that tends to agglomerate into a larger particle (~ 20 nm) [80].

Gold nanoparticle (AuNP) has been formulated into nano aerosol by spark ignition method as a CT contrast agent. Kreyling et al. successfully produced 20 nm-sized AuNP by this method and used radioactive gold ($^{195}$Au) as a material for tracing purposes. An intratracheal inhalation into Wistar-Kyoto rats demonstrated that approximately 30% of AuNP reached the respiratory tract, followed by rapid mucociliary
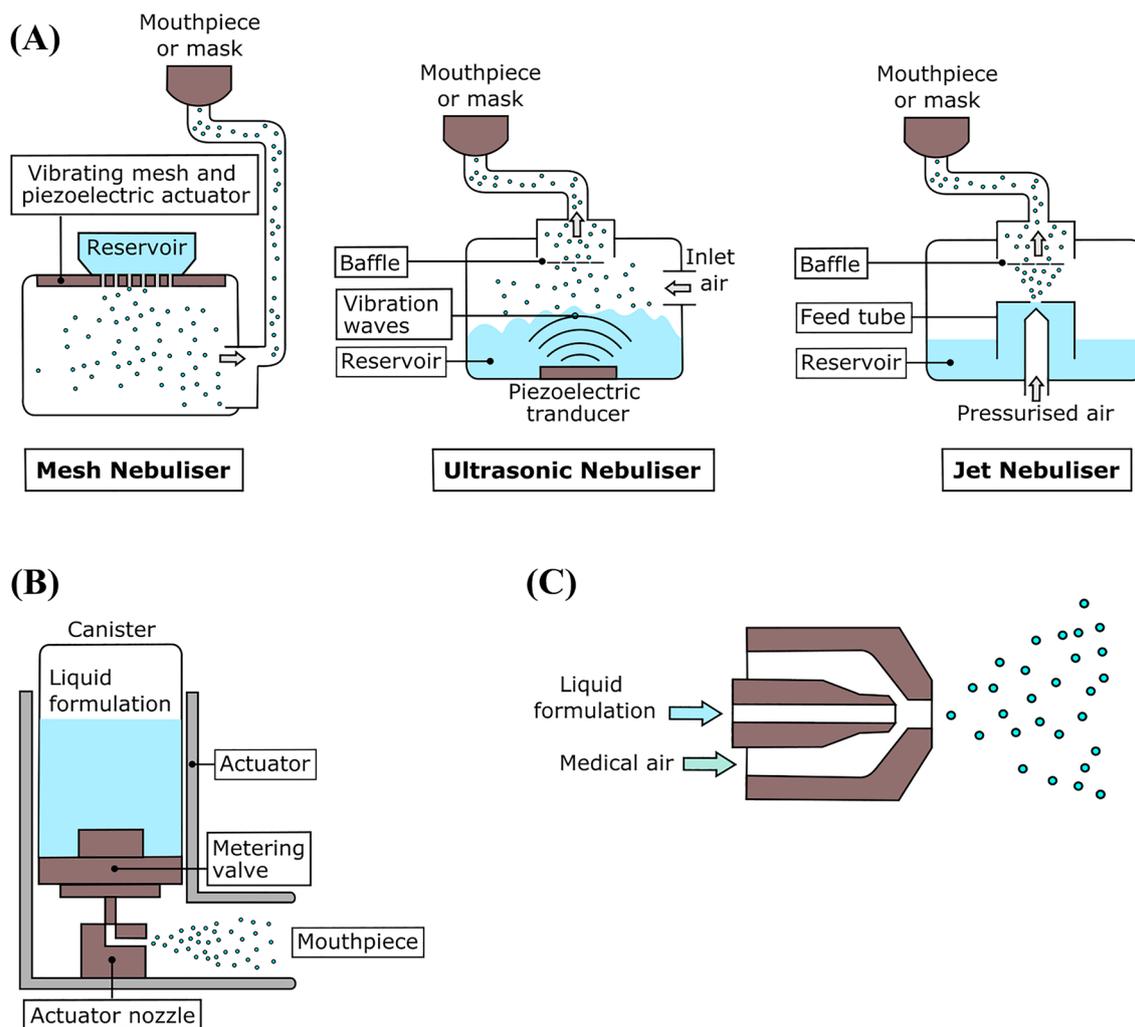


**Fig. 3** Aerosolisation devices for liquid formulation: **A** nebuliser, **B** pressurised-metered dose inhaler (pMDI), **C** air sprayer [114–116]

clearance, and about 80% of AuNP deposited in alveoli was moved from the inner surface into the interstitium within 24 h. Although Kreyling et al. did not perform a CT scan to evaluate the contrast agent performance, the primary deposition of inhaled AuNP in the alveolar region indicates its potential for lung imaging. Nevertheless, an extrapulmonary deposition was also found, mainly in the liver, which increased up to 28 days [33]. Therefore, the toxicity in other organs should be carefully observed to ensure the safety of the AuNP administration.

Another CT contrast agent that has been formulated into nano aerosol by spark ignition is AgNP, which was investigated for its potential toxicity upon inhalation. Campagnolo et al. delivered ~ 25 nm AgNP, generated by spark ignition, into pregnant C57BL/6 female mice via nose-only inhalation, resulting in AgNP accumulation in placentas, albeit very low, and increasing the expression of pregnancy-relevant inflammatory cytokines in the placentas [82]. A biokinetic study of spark-ignited AgNP in Wistar-Kyoto rats administered via tracheal inhalation was also reported by Kreyling et al. Tracing method using radioactive $^{105}AgNP$ showed that $^{105}AgNP$ was mainly excreted via larynx into the gastrointestinal tract due to poor solubility in the lung fluid [83]. These findings imply that the extrapulmonary toxic effect of inhaled AgNP can be minimised by lowering the solubility of the nanoparticle in lung fluid to enhance the mucociliary clearance and reduce the epithelium penetration.

## Spray drying

Spray drying method has been widely investigated for preparing dry powder for drug administration via pulmonary delivery. The ability to incorporate different nanoparticles into size-controllable powder makes spray drying a promising method for developing inhalable powder for lung imaging purposes [54]. In general, spray dryer is classified based on droplet generation and powder collection system. A conventional instrument utilises a gas atomiser and cyclone or bag filter for droplet generation and powder collection, respectively [54]. In a gas atomiser system, the liquid formulation is atomised by pressurised nitrogen gas, in which droplet diameter is affected by the liquid feed and gas flow rate. Droplet diameter can be increased by the increase of feed rate and reduced by increasing the gas flow rate. The cyclone separation system utilises the gravitational force of rotating flow to collect the powder with high inertia [84]. The new instrument, the so-called nano spray dryer, uses a nebuliser to generate droplets and an electrostatic separation system to collect powder [85].

Despite the better particle engineering offered by a nano-spray dryer, only conventional spray dryer type has been utilised for the preparation of an inhalable powder containing $^{99m}Tc$-diethylenetriamine pentaacetic acid

(DTPA) for lung imaging, as reported by Yang et al. in this study, a clinical trial in nine healthy subjects demonstrated that inhaled powder reached lung at 50–70 L/min peak inhalation flow rate. Yang et al. concluded that total and regional lung depositions were not significantly affected by inhaler resistance. Instead, such lung depositions are significantly influenced by inhalation rate and particle size [86]. Despite the success in a clinical trial, the spray drying of radioactive material is a sophisticated process, particularly in avoiding the leakage of radioactive dust from the instrument. It requires tight containment and radioactive material entrapment to ensure the safety of the personnel from radioactive contamination [87]. In contrast, a non-radioactive contrast agent formulation can be carried out using a typical spray dryer without any additional equipment. Furthermore, a combination of different nanoparticles or elements for dual-imaging or theranostic purpose can simply be performed by pre-mixing prior to spray drying, as reported by Julián-López et al. who developed an iron-silica hybrid using a home-made conventional spray dryer [88].

Aside from conventional and nano-spray dryer, supercritical $CO_2$-assisted spray dryer has also been utilised to produce a dry powder with complex structures, such as aerogel. Such a technique allows the material to pass through the supercritical region with the assistance of supercritical fluid, resulting in the absence of interfacial stress [89]. The application of supercritical $CO_2$-assisted spray drying (SASD) for the preparation of inhalable powder containing contrast agents has been reported in the literature.

However, the SASD method poses challenges, including sophisticated instrumentation, high costs, and the presence of organic solvent residuals in the end product [89], which hampers further development in inhalable powder technology [20, 90–92]. For instance, a nanohybrid for dual-imaging consisting of strawberry-like gold-coated magnetite nanocomposites was developed by Silva et al. by SASD method. Using chitosan as a filler, the spray drying process resulted in powder with an aerodynamic diameter of 2.6–2.8 µm and a fine particle fraction (FPF) of 48–55%, which is sufficient for deep lung deposition [20]. Nevertheless, supercritical $CO_2$-assisted spray drying poses challenges, namely high costs, complex instrumentation, and the presence of organic solvent residuals in the end product [89].

Although gold and iron NP are the only investigated contrast agent as inhalable powder via spray drying [90–92], this method is suitable for formulating other contrast or tracing agent into dry powder. The ability to design particle size, structure, and composition makes spray drying a promising method to produce inhalable powder for lung imaging.

## Liquid aerosol

Liquid aerosol for pulmonary delivery is a simpler and cheaper formulation than the dry one. The drug formulation can be dissolved in a suitable solvent, followed by aerosolisation using relatively unsophisticated devices compared to those used for dry aerosol. Another characteristic of liquid aerosol is the immediate solubility upon deposition in the lung airways, avoiding a mucus trap and mucociliary clearance [54]. Therefore, the pulmonary clearance profile of inhaled aerosol is merely affected by the cargo's characteristics, i.e. size and solubility, simplifying the designing process of inhalable particles [93]. Aside from the aforementioned advantages, the application of liquid aerosol in pulmonary delivery also poses challenges, namely the difficulty in aerosol size adjustment and the lower drug stability in liquid formulation compared to that in the dry one [94]. Standard devices used to produce liquid aerosol are nebuliser, pressurised metered-dose inhaler (pMDI), and air spray [55].

## Nebulisation

Nebuliser is the oldest aerosol device and the most widely used for pulmonary drug administration. This device can produce aerosol from liquid formulation using different instrument types, including ultrasonic, jet and vibrating mesh (Fig. 3a). Ultrasonic nebuliser applies high-frequency vibration of the piezoelectric element that transforms liquid formulation into tiny droplets due to sound wave effect. This device type might generate heat upon aerosolisation, which may impact the drug cargo's stability. [93]. A jet nebuliser uses compressed gas that passes through a narrow gap to generate lower pressure and faster gas flow. Subsequently, such a gas flow draws and leads the liquid formulation to hit the baffle for the generation of tiny droplets. Jet nebuliser has two types of valves: the first valve opens during inhalation to increase the aerosol flow, while the second one opens during exhalation for gas release to the atmosphere, avoiding a reverse gas flow. A vibrating mesh nebuliser applies mesh vibration to generate tiny droplets from liquid formulation [55].

To date, nebulisation is the most widely investigated method to deliver contrast or tracing agent via pulmonary delivery for lung imaging, with 31 publications in the past decade (Table 3). Such an extensive investigation of the nebulisation method is most likely due to the simple operating technique during aerosolisation from liquid formulation [93]. This simple method can also be used to aerosolise radioactive material since a commercial nebuliser equipped with the lead container, e.g. SmartVent™, is available for this purpose [95]. Furthermore, different types of nebulisers

lead to dissimilar performance, providing device options to adapt to various drug cargo types [96].

Among different types of nebulisers, a vibrating mesh is the most widely used in clinical or laboratory practice, as seen in Table 3. The reason behind the wide use of vibrating mesh nebulisers has been investigated by Galindo-Filho, et al., where the comparative study of jet and vibrating mesh nebulisers is carried out either in healthy subjects or COPD patients. In healthy subjects, vibrating mesh nebuliser delivered more than twofold $^{99m}$Tc-DTPA into the lung compared to jet nebulisers [96], while in COPD patients, vibrating mesh nebuliser delivered more than threefold $^{99m}$Tc-DTPA into the lung [97]. Galindo-Filho et al. suggested that such a difference is caused by different droplet sizes generated by both nebulisers, where jet and vibrating mesh nebuliser generated droplets with a size of 5 and 3.4 μm [96]. As discussed earlier, a particle size of < 5 μm is essential for deep lung deposition [54]. Aside from comparing different types of nebuliser, a comparative study between $^{99m}$Tc-sulfur colloid powder prepared by Palas rotating brush generator and $^{99m}$Tc-DTPA aerosolised with nebuliser has also been reported in the literature. Kuehl et al. reported that there is no significant difference in both administration methods (6.81–9.08%) since the particle sizes were similar (2.5–2.8 μm) [98].

Table 3 also shows that most of the literature was clinical studies with $^{99m}$Tc-DTPA. It is understandable since $^{99m}$Tc-DTPA is one of the radiopharmaceuticals recommended by the European Association of Nuclear Medicine (EANM) guideline and can easily be administered into the lung [99]. As seen in Table 3, nebulised $^{99m}$Tc-DTPA is mainly used to investigate the effect of particular pulmonary delivery equipment, e.g. positive expiratory pressure device, on the aerosol performance of lung deposition [97, 100–105]. Other studies with $^{99m}$Tc-DTPA focus on distinguishing different lung diseases [74, 106, 107], understanding the physiology of lung disease [108], and investigating the new application of ventilation scintigraphy [109].

Besides the clinical application, nebuliser can also be used for development study of a new contrast agent administration via pulmonary delivery, including AuNP [110], gadolinium nanoparticle (GdNP) [16, 34, 111], Iodine-based contrast agent (I-CA) [18], $MnCl_2$ [112], silver nanoparticle (AgNP) [23, 24], and superparamagnetic iron oxide nanoparticle (SPION) [17, 113]. Such a study aimed to determine lung deposition and clearance [111], investigate biokinetics and toxicity [110, 112], and evaluate the lung image quality generated after inhalation [16, 18].

Despite the simple use of a nebuliser to produce aerosol for pulmonary delivery, this device also has challenges that need to be solved, namely stability issues in liquid formulation and difficulty in particle engineering. The first challenge can be overcome by preparing the drug solution into a

**Table 3** Application and development of nebulisation method for lung imaging in the last decade

| Contrast/tracing agent | Nebuliser type | Research objective | Key finding | References |
|---|---|---|---|---|
| $^{99m}$Tc-sestamibi | Vibrating mesh | Evaluating MRP1 expression in the lung as a result of smoking | Smoking upregulates MRP1 and delays clearance of inhaled Tc-99m-MIB | [95] |
| $^{99m}$Tc-DTPA | — | Investigating aerosol deposition in ferrets' lung | The respiratory tract deposition was ~9% for liquid formulation and 5–6% for the dry one. The lung deposition in both formulations were similar | [98] |
| $^{99m}$Tc-DTPA | — | Evaluation the use of V/Q scintigraphy as an alternative modality for diagnosis in patients with bronchopleural fistula | bronchoscopy or the methylene blue test failed to identify residual air leak detected by V/Q scintigraphy | [109] |
| $^{99m}$Tc-sestamibi/DTPA/MDP | — | Comparing the use of $^{99m}$Tc-sestamibi, $^{99m}$Tc-DTPA, and $^{99m}$Tc-MDP in P/Q scintigraphy to asses pulmonary thromboembolism | $^{99m}$Tc-sestamibi demonstrated the highest count rate, the slowest alveolar clearance, and the best quality image | [117] |
| $^{99m}$Tc-nanocarbon or $^{99m}$Tc-DTPA | — | Evaluating the occurrence of COPD in patients suspected PE using V/Q scintigraphy and investigating the performance of V/Q scintigraphy to diagnose PE in patients with COPD | PE was diagnosed in 353 (28%) patients. Mild, moderate or severe airway obstruction were shown in 697 patients (55%). Among patients with PE, 90 patients (25%) were also diagnosed as COPD | [74] |
| $^{99m}$Tc-DTPA | — | examination alveolar fluid clearance in CHF patients compared against healthy controls | A significantly faster alveolar fluid clearance was observed in CHF patients than controls | [108] |
| $^{99m}$Tc-sulfur colloid | Jet | Evaluating the aerosol deposition and mucociliary clearance following Ivacaftor treatment in Cystic Fibrosis | The homogeneity improvement was observed, indicated by a decrease in number ratio of pixels with higher and lower deposition. Mucociliary clearance also increased | [118] |
| $^{99m}$Tc-arginine | Jet | Evaluation the deposition of $^{99m}$Tc-arginine in the lung for COPD therapy | 15 ± 2% of aerosolised $^{99m}$Tc-arginine was deposited in the lung | [119] |
| $^{99m}$Tc-sestamibi | Vibrating mesh | Investigating the correlation between $^{99m}$Tc-sestamibi clearance and MRP1 expression | $^{99m}$Tc- sestamibi clearance was faster in patients with low MRP1 expression compared with those with higher MRP1 expression | [120] |
| $^{99m}$Tc-DTPA | Vibrating | Comparing lung deposition in two invasive mechanical ventilation: pressure support ventilation and volume-controlled ventilation | The lung deposition for pressure support and volume-controlled ventilation was 10.5 ± 3.0 and 15.1 ± 5.0%, respectively. Pressure support ventilation demonstrated higher endotracheal tube and tracheal deposition | [101] |
| $^{99m}$Tc-DTPA | — | Evaluating the effect of positive expiratory pressure on $^{99m}$Tc-DTPA clearance | $^{99m}$Tc-DTPA clearance was significantly faster with the presence of positive expiratory pressure | [102] |
| $^{99m}$Tc-sulfur colloid | Vibrating mesh | Evaluating the effect of posture (supine and seated) on lung deposition | $^{99m}$Tc-sulfur colloid deposition in the alveolar region for supine was significantly lower than for seated. The deposition in the intermediate region and small airways for supine was significantly higher than for seated | [121] |
| $^{99m}$Tc-DTPA | Jet | Comparing lung deposition after central and peripheral administration | There was no significant difference in lung deposition after central and peripheral administration | [103] |
| $^{99m}$Tc-DTPA | Vibrating mesh | Evaluating whether $^{99m}$Tc-DTPA can distinguish asthma and COPD | The $T_{1/2}$ values of $^{99m}$Tc-DTP of the non-smoking COPD patients were significantly lower than non-smoking asthma patients. The cap value was significantly higher in non-smoking COPD patients | [106] |

**Table 3** (continued)

| Contrast/tracing agent | Nebuliser type | Research objective | Key finding | References |
|---|---|---|---|---|
| $^{99m}$Tc-tin colloid | – | Comparing the effect of Laerdal and Mapleson-C circuits for positive end-expiratory pressure setting on the lung deposition | Aerosol deposition was higher in the right lung region than in the left one, and the lowest deposition was observed in the left lower region | [122] |
| $^{99m}$Tc-DTPA | Ultrasound | Evaluating the application of low dose CT to distinguish between COPD and PE during V/Q SPECT/CT | The mean lung tissue density in healthy areas was 758 HU, in V/Q mismatch defects (PE) 695 HU, and in V/Q match defects (COPD) 900 HU | [107] |
| $^{99m}$Tc-DTPA | – | Investigating the influence of continuous positive airway pressure and body position on the lung clearance | 20 cmH$_2$O of air pressure significantly reduced the lung clearance in the supine and seated positions. However, 10 cmH$_2$O air pressure did not affect the lung clearance in both positions | [100] |
| $^{99m}$Tc-DTPA | Jet and vibrating mesh | Comparing the performance jet and vibrating mesh nebuliser in healthy subjects | Vibrating mesh nebulisers delivered more than twofold $^{99m}$Tc-DTPA into the lung compared to jet nebulisers | [96] |
| $^{99m}$Tc-DTPA | Jet | Investigating the effect of Acapella positive expiratory pressure device and nebuliser configuration on the lung deposition | Administration without Acapella and with nebuliser in between Acapella and patient resulted in higher lung deposition than setting the nebuliser distal to the Acapella | [104] |
| $^{99m}$Tc-DTPA | Jet and vibrating mesh | Comparing the performance jet and vibrating mesh nebuliser coupled with NIV in COPD patients | Vibrating mesh nebulisers delivered more than threefold $^{99m}$Tc-DTPA into the lung compared to jet nebulisers | [97] |
| $^{99m}$Tc-DTPA | Jet | Investigating the effect of NIV coupling on the lung deposition in the asthma patients | The application of NIV upon nebulisation did not improve the lung deposition of $^{99m}$Tc-DTPA | [105] |
| NH$_2$-(PVA/PEG) AuNPs | Vibrating mesh | Investigation of aerosolised AuNPs functionalised with NH$_2$PVA and NH$_2$-PEG | Accumulation in macrophages (20%), epithelial (60%), and dendritic cells (20%) was observed after repeated aerosolisation. No cytotoxicity and proinflammation were shown but significant apoptosis was observed after 96 h | [110] |
| AgNP | Jet | Documenting the kinetic time course of inhaled Ag NPs with size of 20 nm | Only small percentage of aerosol reached the lung (1–2.5%) since most of the aerosol were retained in the upper airways. AgNP was also found in gastrointestinal tract, liver, lymphatic node, OB, kidney, and spleen, 6 h following the onset of inhalation | [23] |
| AgNP with a size of 20 or 110 nm | Jet collision | Evaluating: the deposition and retention of AgNP in the nasal cavity; the translocation and retention time of AgNP in the OB; and the effect of AgNP in the OB on the activity of microglial cells | The highest nasal deposition was found immediately after AgNP deposition in the nose, translocation rate to the brain, and subsequent microglial activation in the OB was affected by AgNP size and time after inhalation | [24] |
| SPIONs | Jet | Pysicochemical characterisation of SPIONs aerosol | The aerosol size measured by TEM, PCS, NTA, impinger, and SMPS was $9 \pm 2$, $27 \pm 7$, $56 \pm 10$, $159 \pm 46$, and 75 nm, respectively | [113] |
| SPIONs | Vibrating mesh | Development of MPI for inhaled aerosol tracking and quantification | SPIONs have potential as highly sensitive tracer for lung imaging and theranostic agent via magnetic actuation or hyperthermia effect | [17] |

**Table 3** (continued)

| Contrast/tracing agent | Nebuliser type | Research objective | Key finding | References |
|---|---|---|---|---|
| Gd-DOTA | Jet | evaluating the performance of UTE sequences for imaging and quantifying the deposition of inhaled Gd-DOTA | 3D acquisitions with isotropic millimetric resolution were obtained rapidly. Images demonstrated homogeneous and significant signal enhancement (> 200%). The visualisation of deposited Gd-DOTA in the level of the bronchi of secondary lobules was obtained | [16] |
| Gd-DOTA | – | aerosol deposition and to characterize signal enhancement in asthmatic rat lungs | A lower signal enhancement and deposited aerosol were observed in asthmatic model rats. Approximately 1 μmol/kg body weight in the standard clinical MRI has potential application for asthma diagnosis | [34] |
| Gd-DOTA (gadoterate meglumine) | Jet | Evaluating the performance of UTE sequences for quantifying the deposition of inhaled Gd-DOTA | In the lung parenchyma, 50% signal enhancement was observed. Gd-DOTA clearance was 14% per h and Gd-DOTA deposition was homogeneous in the lung | [111] |
| $MnCl_2$ | – | Investigating the effectiveness of $MnCl_2$ on targeting adenocarcinoma and its toxicity | Tumours of submillimeter size can be identified by pulmonary delivery of $MnCl_2$ with dose of 20 times lower than that of systemic. No $Mn^{2+}$ was detected in the brain and liver | [112] |
| Iodine-based liquid (Ultravist-370) | Vibrating mesh | Exploring the use of dynamic X-ray phase-contrast imaging to observe pulmonary drug delivery | Only 8% of liquid reached the lung. Temporal resolution was up to 1.5 fps | [18] |

AgNP, silver nanoparticle; AuNP, gold nanoparticle; CHF, chronic heart failure; COPD, chronic obstructive pulmonary disease; DOTA, dodecane tetraacetic acid; DTPA, diethylenetriamine-pentaacetic acid; HU, Hounsfield units; MDP, methylene diphosphonate; MPI, magnetic particle imaging; MRPI, multidrug resistance protein-1; NIV, non-invasive ventilation; OB, olfactory bulb; PE, pulmonary embolism; PEG, polyethylene glycol; PVA, polyvinyl alcohol; SPIONs, super paramagnetic iron oxide nanoparticles; $^{99m}$Tc, Technetium-99m

lyophilised formulation that can be rehydrated prior to use. Such a lyophilisation method has been applied in radiopharmaceutical kits formulation that can be rehydrated and radiolabelled by [99mTc]-pertechnetate in saline solution [94]. Therefore, this method can also be applied in the development of other contrast and tracing agents. Another challenge is the limitation of the nebuliser in particle engineering, unlike spray drying, which can easily design the inhalable powder, e.g. size and porosity [54].

### Pressurised metered-dose inhaler (pMDI)

Pressurised metered-dose inhaler (pMDI) releases liquid formulation mixed with propellant from a pressurised canister, allowing droplets generation for aerosol inhalation (Fig. 3b) [123]. Due to the portable size and simplicity of use, patients can use pMDIs for inhalation treatment without any help from a medical worker [115]. The main drawback of pMDI is the incompatibility of particular drug cargo with the propellant mixture or pressurised storage. To date, [99mTc]-labelled radiopharmaceutical is the only substance administered by pMDI for investigating the lung deposition of particular drugs and the performance of additional equipment for pulmonary delivery [123–126].

Radiotracing studies of pMDI-delivered aerosol revealed that lung deposition is influenced by the aerosol size, liquid formulation, and additional inhalation equipment. Clinical study of pMDI-aerosolised Beclomethasone and Fluticasone with hydrofluoroalkane (HFA) as a propellant in patients with asthma has been reported by Leach et al. This study demonstrated that the lung deposition of [99mTc]-Beclomethasone was significantly higher than that of [99mTc]-Fluticasone (55 vs. 24%), which can be explained by the difference of aerosol size (0.7 vs. 2.0 µm) [126]. A study reported by Ditcham et al. demonstrated that the deposition of inhaled [99mTc]-Albuterol aerosol with a facemask was higher (18.1%) than that with a spacer mouthpiece (22.5%) [123]. A study comparing the lung deposition of radiolabelled drug-aerosol in healthy subjects and patients with asthma reported that the deposition patterns were similar in healthy and people with asthma (22–25%) [124]. Nevertheless, the lung deposition of pMDI-aerosol might be different in other lung diseases, as observed in a study using aerosol generated by other devices [13, 74].

Although the development of a pMDI-aerosolised contrast agent has not been reported, the delivery of nanostructured particles via pMDI is feasible, as reported by Taylor et al., where glycopyrronium/formoterol fumarate or phospholipid porous particles was [99mTc]-radiolabelled and administered via pMDI into five healthy male subjects. A gamma scintigraphy assessment revealed that 38.4% of emitted dose reached the lung, 61.4% was detected in the oropharyngeal and stomach, and <0.25% of the emitted dose was detected in the exhalation filter [125].

### Air spray

The last method that has been investigated for the delivery of an inhalable tracing agent is air spraying method, which is similar to the atomisation method used in spray dryer for droplet generation. In brief, pressurised medical air and pumped liquid formulation are applied to generate an atomising flow of 0.5 L min$^{-1}$ with a median particle size distribution of 40–60 µm. Although such a distribution range is theoretically too large for desirable lung deposition, the preclinical study of [99mTc]-labelled porcine surfactant in six sedated 1-day-old piglets nasal-mask continuous positive pressure airway demonstrated 40% lung deposition after 28 min inhalation [116]. Such relatively high lung deposition compared to other aerosolisation methods, such as nebulisation [101, 119], can be due to the difference in an animal model or the presence of a continuous positive pressure airway [104]. Therefore, a comparative study should be performed between air spray and other nebulisation methods with identical experimental conditions to compare better.

## Conclusion and future perspective

The use of contrast and tracing agent in lung imaging has been applied in the last decades, with 38 commercially available products. A high surface area, non-invasive administration, the potential to avoid extrapulmonary toxicity, and the availability of various administration devices make pulmonary delivery the best option for administering contrast and tracing agents to obtain optimal image quality. The key performance parameter of inhalable aerosol is the particle size affecting the lung deposition and clearance, eventually determining the image quality and toxicity profile, respectively. Another critical parameter of inhaled contrast and tracing agents is the elemental form, such as ionic or nanoparticle form, affecting the lung clearance profile. The research outputs reviewed here show that different aerosolisation methods are suitable depending on the characteristics of contrast and tracing agents, such as the graphite ablation method for a radionuclide-based tracing agent. Nevertheless, graphite ablation and nebulisation are the most widely used aerosolisation method for dry and liquid aerosol production, respectively.

Further development of aerosol delivery for lung imaging should also consider the combination of more than one element to improve the image quality or provide a dual-imaging modality. For instance, the combination of Fe and Au provides a dual contrast agent using MRI and CT scans. Such a combination can be prepared upon preparing nanoparticles,

resulting in dual elements nanoparticle, or combined upon aerosol preparation, such as during spray drying. The latter method can be performed easily since the combination of available formulas is feasible as long as the formulas are compatible. Another further development of new aerosol for lung imaging is using an animal model, which mainly focuses on small animals, such as a mouse. Due to the distant physiological and anatomical gap between the animal model and human lung, the use of small animals in pre-clinical study typically has low translational success. Therefore, the use of relatively larger animals, such as piglets or ferrets, should be considered in future studies.

## Declarations

**Conflict of interest** All authors declare that they have no conflict of interest.

**Ethical approval** Not applicable.

## References

1. Gedebjerg A, Szépligeti SK, Wackerhausen LMH et al (2018) Prediction of mortality in patients with chronic obstructive pulmonary disease with the new Global Initiative for Chronic Obstructive Lung Disease 2017 classification: a cohort study. Lancet Respir Med 6:204–212. https://doi.org/10.1016/S2213-2600(18)30002-X

2. Amaral AFS, Patel J, Kato BS et al (2018) Airflow obstruction and use of solid fuels for cooking or heating BOLD (Burden of Obstructive Lung Disease) results. Am J Respir Crit Care Med 197:595–610. https://doi.org/10.1164/rccm.201701-0205OC

3. Ratnatunga CN, Lutzky VP, Kupz A et al (2020) The rise of non-tuberculosis mycobacterial lung disease. Front Immunol 11:1

4. Sunjaya AP, Allida SM, di Tanna GL, Jenkins CR (2021) Asthma and coronavirus disease 2019 risk: a systematic review and meta-analysis. Eur Respir J. https://doi.org/10.1183/13993003.01209-2021

5. Sleeman KE, de Brito M, Etkind S et al (2019) The escalating global burden of serious health-related suffering: projections to 2060 by world regions, age groups, and health conditions. Lancet Glob Health 7:e883–e892. https://doi.org/10.1016/S2214-109X(19)30172-X

6. Gershon AS, Thiruchelvam D, Chapman KR et al (2018) Health services burden of undiagnosed and overdiagnosed COPD. Chest 153:1336–1346. https://doi.org/10.1016/j.chest.2018.01.038

7. Diab N, Gershon AS, Sin DD et al (2018) Underdiagnosis and overdiagnosis of chronic obstructive pulmonary disease. Am J Respir Crit Care Med 198:1130–1139

8. Spyratos D, Chloros D, Michalopoulou D, Sichletidis L (2016) Estimating the extent and economic impact of under and over-diagnosis of chronic obstructive pulmonary disease in primary care. Chron Respir Dis 13:240–246. https://doi.org/10.1177/1479972316636989

9. Prabhakar B, Shende P, Augustine S (2018) Current trends and emerging diagnostic techniques for lung cancer. Biomed Pharmacother 106:1586–1599

10. le Roux PY, Robin P, Salaun PY (2018) New developments and future challenges of nuclear medicine and molecular imaging for pulmonary embolism. Thromb Res 163:236–241. https://doi.org/10.1016/j.thromres.2017.06.031

11. Semenov S (2009) Microwave tomography: review of the progress towards clinical applications. Philos Trans R Soc A Math Phys Eng Sci 367:3021–3042

12. Darquenne C, Fleming JS, Katz I et al (2016) Bridging the gap between science and clinical efficacy: physiology, imaging, and modeling of aerosols in the lung. J Aerosol Med Pulm Drug Deliv 29:107–126. https://doi.org/10.1089/jamp.2015.1270

13. Currie GM, Bailey DL (2021) A technical overview of technegas as a lung ventilation agent. J Nucl Med Technol 49:313–319. https://doi.org/10.2967/jnmt.121.262887

14. Cao Y, Xu L, Kuang Y et al (2017) Gadolinium-based nanoscale MRI contrast agents for tumor imaging. J Mater Chem B 5:3431–3461

15. Koç MM, Aslan N, Kao AP, Barber AH (2019) Evaluation of X-ray tomography contrast agents: a review of production, protocols, and biological applications. Microsc Res Tech 82:812–848

16. Crémillieux Y, Montigaud Y, Bal C et al (2020) Three-dimensional quantitative MRI of aerosolized gadolinium-based nanoparticles and contrast agents in isolated ventilated porcine lungs. Magn Reson Med 83:1774–1782. https://doi.org/10.1002/mrm.28041

17. Tay ZW, Chandrasekharan P, Zhou XY et al (2018) In vivo tracking and quantification of inhaled aerosol using magnetic particle imaging towards inhaled therapeutic monitoring. Theranostics 8:3676–3687. https://doi.org/10.7150/thno.26608

18. Gradl R, Dierolf M, Yang L et al (2019) Visualizing treatment delivery and deposition in mouse lungs using in vivo X-ray imaging. J Control Release 307:282–291. https://doi.org/10.1016/j.jconrel.2019.06.035

19. Rathmann SM, Ahmad Z, Slikboer S et al (2019) The radiopharmaceutical chemistry of Technetium-99m. In: Radiopharmaceutical chemistry. Springer, New York, pp 311–333

20. Silva MC, Silva AS, Fernandez-Lodeiro J et al (2017) Supercritical $CO_2$-assisted spray drying of strawberry-like gold-coated magnetite nanocomposites in chitosan powders for inhalation. Materials. https://doi.org/10.3390/ma10010074

21. Huynh M, Kempson I, Bezak E, Phillips W (2021) Predictive modeling of hypoxic head and neck cancers during fractionated radiotherapy with gold nanoparticle radiosensitization. Med Phys 48:3120–3133. https://doi.org/10.1002/mp.14872

22. Mahan MM, Doiron AL (2018) Gold nanoparticles as X-ray, CT, and multimodal imaging contrast agents: formulation, targeting, and methodology. J Nanomater 1:1

23. Andriamasinoro SN, Dieme D, Marie-Desvergne C et al (2022) Kinetic time courses of inhaled silver nanoparticles in rats. Arch Toxicol 96:487–498. https://doi.org/10.1007/s00204-021-03191-0

24. Patchin ES, Anderson DS, Silva RM et al (2016) Size-dependent deposition, translocation, and microglial activation of inhaled silver nanoparticles in the rodent nose and brain. Environ Health Perspect 124:1870–1875. https://doi.org/10.1289/EHP234

25. Bulte JWM (2019) Superparamagnetic iron oxides as MPI tracers: a primer and review of early applications. Adv Drug Deliv Rev 138:293–301

26. Morgan J, Bell R, Jones AL (2020) Endogenous doesn't always mean innocuous: a scoping review of iron toxicity by inhalation. J Toxicol Environ Health B Crit Rev 23:107–136

27. Martínez-Rovira I, Seksek O, Puxeu J et al (2019) Synchrotron-based infrared microspectroscopy study on the radiosensitization effects of Gd nanoparticles at megavoltage radiation energies. Analyst 144:5511–5520. https://doi.org/10.1039/c9an00792j

28. Sobańska Z, Roszak J, Kowalczyk K, Stępnik M (2021) Applications and biological activity of nanoparticles of manganese and manganese oxides in in vitro and in vivo models. Nanomaterials 11:1

29. Cai X, Zhu Q, Zeng Y et al (2019) Manganese oxide nanoparticles as mri contrast agents in tumor multimodal imaging and therapy. Int J Nanomedicine 14:8321–8344

30. Zhang P, Ma X, Guo R et al (2021) Organic nanoplatforms for iodinated contrast media in CT imaging. Molecules 26:1

31. Lusic H, Grinstaff MW (2013) X-ray-computed tomography contrast agents. Chem Rev 113:1641–1666

32. Caspani S, Magalhães R, Araújo JP, Sousa CT (2020) Magnetic nanomaterials as contrast agents for MRI. Materials 13:1

33. Kreyling WG, Möller W, Holzwarth U et al (2018) Age-dependent rat lung deposition patterns of inhaled 20 nanometer gold nanoparticles and their quantitative biokinetics in adult rats. ACS Nano 12:7771–7790. https://doi.org/10.1021/acsnano.8b01826

34. Wang H, Sebrié C, Judé S et al (2018) Quantitative Gd-DOTA-based aerosol deposition mapping in the lungs of asthmatic rats using 3D UTE-MRI. NMR Biomed. https://doi.org/10.1002/nbm.4013

35. Ni D, Bu W, Ehlerding EB et al (2017) Engineering of inorganic nanoparticles as magnetic resonance imaging contrast agents. Chem Soc Rev 46:7438–7468

36. Zhou Z, Bai R, Munasinghe J et al (2017) T1–T2 dual-modal magnetic resonance imaging: from molecular basis to contrast agents. ACS Nano 11:5227–5232

37. Volpi S, Ali JM, Tasker A et al (2018) The role of positron emission tomography in the diagnosis, staging and response assessment of non-small cell lung cancer. Ann Transl Med 6:95–95. https://doi.org/10.21037/atm.2018.01.25

38. Bajc M, Lindqvist A (2019) Ventilation/perfusion SPECT imaging—diagnosing other cardiopulmonary diseases beyond pulmonary embolism. Semin Nucl Med 49:4–10

39. Sanchez-Crespo A (2019) Lung scintigraphy in the assessment of aerosol deposition and clearance. Semin Nucl Med 49:47–57

40. Munir M, Sriyono A et al (2020) Development of mesoporous γ-alumina from aluminium foil waste for 99Mo/99mTc generator. J Radioanal Nucl Chem 326:87–96. https://doi.org/10.1007/s10967-020-07288-1

41. Blanc-Béguin F, Eliès P, Robin P et al (2021) 68Ga-labelled carbon nanoparticles for ventilation PET/CT imaging: physical properties study and comparison with technegas®. Mol Imaging Biol 23:62–69. https://doi.org/10.1007/s11307-020-01532-6

42. Tan AEH, Pua U (2010) Thyroid uptake of technegas during V/Q scintigraphy in graves disease. Am J Med 123:1

43. Meher BR, Agrawal K, Gnanasegaran G (2021) Review of adverse reactions associated with the use of common diagnostic radiopharmaceuticals. Indian J Nucl Med 36:163–167

44. Miranda ACC, Durante ACR, Fuscaldi LL, de Barboza MF (2019) Current approach in radiochemical quality control of the 99mTc-radiopharmaceuticals: a mini-review. Braz Arch Biol Technol 62:1–7

45. Vogt ACS, Arsiwala T, Mohsen M et al (2021) On iron metabolism and its regulation. Int J Mol Sci 22:1

46. de Berardis B, Marchetti M, Risuglia A et al (2020) Exposure to airborne gold nanoparticles: a review of current toxicological data on the respiratory tract. J Nanopart Res 22:1

47. Hadrup N, Sharma AK, Loeschner K, Jacobsen NR (2020) Pulmonary toxicity of silver vapours, nanoparticles and fine dusts: a review. Regul Toxicol Pharmacol 115:1

48. Do C, DeAguero J, Brearley A et al (2020) Gadolinium-based contrast agent use, their safety, and practice evolution. Kidney360 1:561–568. https://doi.org/10.34067/kid.0000272019

49. Foroozandeh P, Aziz AA (2018) Insight into cellular uptake and intracellular trafficking of nanoparticles. Nanoscale Res Lett. https://doi.org/10.1186/s11671-018-2728-6

50. Allden SJ, Ogger PP, Ghai P et al (2019) The transferrin receptor CD71 delineates functionally distinct airway macrophage subsets during idiopathic pulmonary fibrosis. Am J Respir Crit Care Med 200:209–219. https://doi.org/10.1164/rccm.201809-1775OC

51. Brudecki K, Borkowska E, Gorzkiewicz K et al (2019) 99mTc activity concentrations in room air and resulting internal contamination of medical personnel during ventilation–perfusion lung scans. Radiat Environ Biophys 58:469–475. https://doi.org/10.1007/s00411-019-00793-2

52. Avison M, Hart G (2001) The use of a modified technique to reduce radioactive air contamination in aerosol lung ventilation imaging. J Radiol Protect 21:155

53. Darquenne C (2012) Aerosol deposition in health and disease. J Aerosol Med Pulm Drug Deliv 25:140–147

54. Munir M, Jena L, Kett VL et al (2021) Spray drying: inhalable powders for pulmonary gene therapy. Mater Sci Eng, C. https://doi.org/10.1016/j.msec.2021.112601

55. Gaul R, Ramsey JM, Heise A et al (2018) Nanotechnology approaches to pulmonary drug delivery: targeted delivery of small molecule and gene-based therapeutics to the lung. In: Design of nanostructures for versatile therapeutic applications. Elsevier, New York, pp 221–253

56. Brown JS, Zeman KL, Bennett WD (2001) Regional deposition of coarse particles and ventilation distribution in healthy subjects and patients with cystic fibrosis. Mary Ann Liebert, Inc., London

57. Füri P, Hofmann W, Jókay Á et al (2017) Comparison of airway deposition distributions of particles in healthy and diseased workers in an Egyptian industrial site. Inhal Toxicol 29:147–159. https://doi.org/10.1080/08958378.2017.1326990

58. Löndahl J, Swietlicki E, Rissler J et al (2012) Experimental determination of the respiratory tract deposition of diesel combustion particles in patients with chronic obstructive pulmonary disease. Part Fibre Toxicol. https://doi.org/10.1186/1743-8977-9-30

59. Aaltonen HL, Jakobsson JK, Diaz S et al (2018) Deposition of inhaled nanoparticles is reduced in subjects with COPD and correlates with the extent of emphysema: proof of concept for a novel diagnostic technique. Clin Physiol Funct Imaging 38:1008–1014. https://doi.org/10.1111/cpf.12517

60. Jakobsson JKF, Aaltonen HL, Nicklasson H et al (2018) Altered deposition of inhaled nanoparticles in subjects with chronic obstructive pulmonary disease. BMC Pulm Med. https://doi.org/10.1186/s12890-018-0697-2

61. Brand P, Schulte M, Wencker M et al (2008) Lung deposition of inhaled α1-proteinase inhibitor in cystic fibrosis and α1-antitrypsin deficiency. Eur Respir J 34:354–360. https://doi.org/10.1183/09031936.00118408

62. Schwarz C, Procaccianti C, Mignot B et al (2021) Deposition of inhaled levofloxacin in cystic fibrosis lungs assessed by functional respiratory imaging. Pharmaceutics. https://doi.org/10.3390/pharmaceutics13122051

63. Lenney W, Edenborough F, Kho P, Kovarik JM (2011) Lung deposition of inhaled tobramycin with eFlow rapid/LC Plus jet nebuliser in healthy and cystic fibrosis subjects. J Cyst Fibros 10:9–14. https://doi.org/10.1016/j.jcf.2010.08.019

64. Jakobsson JKF, Hedlund J, Kumlin J et al (2016) A new method for measuring lung deposition efficiency of airborne

nanoparticles in a single breath. Sci Rep 6:1–10. https://doi.org/10.1038/srep36147

65. Möller W, Felten K, Sommerer K et al (2008) Deposition, retention, and translocation of ultrafine particles from the central airways and lung periphery. Am J Respir Crit Care Med 177:426–432. https://doi.org/10.1164/rccm.200602-301OC

66. Chalupa DC, Morrow PE, Oberdörster G et al (2004) Ultrafine particle deposition in subjects with asthma. Environ Health Perspect 112:879–882. https://doi.org/10.1289/ehp.6851

67. Farkas Á, Lizal F, Jedelsky J et al (2020) The role of the combined use of experimental and computational methods in revealing the differences between the micron-size particle deposition patterns in healthy and asthmatic subjects. J Aerosol Sci. https://doi.org/10.1016/j.jaerosci.2020.105582

68. Virchow JC, Poli G, Herpich C et al (2018) Lung deposition of the dry powder fixed combination beclometasone dipropionate plus formoterol fumarate using NEXThaler® device in healthy subjects, asthmatic patients, and COPD patients. J Aerosol Med Pulm Drug Deliv 31:269–280. https://doi.org/10.1089/jamp.2016.1359

69. Anderson PJ, Wilson JD, Hiller FC (1990) Respiratory tract deposition of ultrafine particles in subjects with obstructive or restrictive lung disease. Chest 97:1115–1120. https://doi.org/10.1378/chest.97.5.1115

70. Verger A, Bahloul A, Melki S et al (2020) Tracheobronchitis signs observed on ventilation lung scintigraphy during the course of COVID-19 infection. Eur J Nucl Med Mol Imaging 47:2709–2710

71. Wiebe IL, Burch MW, Abrams ND (2010) Review: Technegas-99mTc-metal core graphite nanoparticles for pulmonary ventilation imaging. Curr Radiopharmaceut 3:49–59. https://doi.org/10.2174/1874471011003010049

72. Mills NL, Amin N, Robinson SD et al (2006) Do inhaled carbon nanoparticles translocate directly into the circulation in humans? Am J Respir Crit Care Med 173:426–431. https://doi.org/10.1164/rccm.200506-865OC

73. Senden TJ, Moock KH, Gerald JF et al (1997) The physical and chemical nature of technegas. J Nucl Med 38:1327–1333

74. Nasr A, Lindqvist A, Bajc M (2017) Ventilation defect typical for COPD is frequent among patients suspected for pulmonary embolism but does not prevent the diagnosis of PE by V/P SPECT. EC Pulmonol Respir Med 4:85–91

75. le Roux PY, Palard X, Robin P et al (2014) Safety of ventilation/perfusion single photon emission computed tomography for pulmonary embolism diagnosis. Eur J Nucl Med Mol Imaging 41:1957–1964. https://doi.org/10.1007/s00259-014-2763-1

76. Zhang M, Yang M, Morimoto T et al (2018) Size-dependent cell uptake of carbon nanotubes by macrophages: a comparative and quantitative study. Carbon N Y 127:93–101. https://doi.org/10.1016/j.carbon.2017.10.085

77. Pacurari M, Lowe K, Tchounwou PB, Kafoury R (2016) A review on the respiratory system toxicity of carbon nanoparticles. Int J Environ Res Public Health 13:1

78. Mortensen J, Berg RMG (2018) Lung scintigraphy in COPD. Semin Nucl Med 49:16–21. https://doi.org/10.1053/j.semnuclmed.2018.10.010

79. Pinho DF, Banga A, Torres F, Mathews D (2019) Ventilation perfusion pulmonary scintigraphy in the evaluation of pre-and post-lung transplant patients. Transplant Rev 33:107–114. https://doi.org/10.1016/j.trre.2018.10.003

80. Pfeiffer T, Feng J, Schmidt-Ott A (2014) New developments in spark production of nanoparticles. Adv Powder Technol 25:56–70

81. Gautam M, Kim JO, Yong CS (2021) Fabrication of aerosol-based nanoparticles and their applications in biomedical fields. J Pharm Investig 51:361–375

82. Campagnolo L, Massimiani M, Vecchione L et al (2017) Silver nanoparticles inhaled during pregnancy reach and affect the placenta and the foetus. Nanotoxicology 11:687–698. https://doi.org/10.1080/17435390.2017.1343875

83. Kreyling WG, Holzwarth U, Hirn S et al (2020) Quantitative biokinetics over a 28 day period of freshly generated, pristine, 20 nm silver nanoparticle aerosols in healthy adult rats after a single 1½-hour inhalation exposure. Part Fibre Toxicol. https://doi.org/10.1186/s12989-020-00347-1

84. Emami F, Vatanara A, Park EJ, Na DH (2018) Drying technologies for the stability and bioavailability of biopharmaceuticals. Pharmaceutics 10:1–22. https://doi.org/10.3390/pharmaceutics10030131

85. Munir M, Kett VL, Dunne NJ, McCarthy HO (2022) Development of a spray-dried formulation of peptide-DNA nanoparticles into a dry powder for pulmonary delivery using factorial design. Pharm Res. https://doi.org/10.1007/s11095-022-03256-4

86. Yang MY, Verschuer J, Shi Y et al (2016) The effect of device resistance and inhalation flow rate on the lung deposition of orally inhaled mannitol dry powder. Int J Pharm 513:294–301. https://doi.org/10.1016/j.ijpharm.2016.09.047

87. Zuckier LS, Moadel RM, Haramati LB, Freeman LM (2020) Diagnostic evaluation of pulmonary embolism during the COVID-19 pandemic. J Nucl Med 61:630–631. https://doi.org/10.2967/jnumed.120.245571

88. Julián-López B, Boissière C, Chanéac C et al (2007) Mesoporous maghemite-organosilica microspheres: a promising route towards multifunctional platforms for smart diagnosis and therapy. J Mater Chem 17:1563–1569. https://doi.org/10.1039/b615951f

89. Badens E, Masmoudi Y, Mouahid A, Crampon C (2018) Current situation and perspectives in drug formulation by using supercritical fluid technology. J Supercrit Fluids 134:274–283. https://doi.org/10.1016/j.supflu.2017.12.038

90. Silva AS, Sousa AM, Cabral RP et al (2017) Aerosolizable gold nano-in-micro dry powder formulations for theragnosis and lung delivery. Int J Pharm 519:240–249. https://doi.org/10.1016/j.ijpharm.2017.01.032

91. Kronawitt J, Fan Z, Schöttle M et al (2019) Redispersible gold nanoparticle/polymer composite powders ready for ligand exchange reactions. ChemNanoMat 5:181–186. https://doi.org/10.1002/cnma.201800517

92. Diem PHN, Thao DTT, van Phu D et al (2017) Synthesis of gold nanoparticles stabilized in dextran solution by gamma Co-60 ray irradiation and preparation of gold nanoparticles/dextran powder. J Chem. https://doi.org/10.1155/2017/6836375

93. Gomes dos Reis L, Svolos M, Hartwig B et al (2017) Inhaled gene delivery: a formulation and delivery approach. Expert Opin Drug Deliv 14:319–330. https://doi.org/10.1080/17425247.2016.1214569

94. Bjeloševic M, Zvonar Pobirk A, Planinšek O, Ahlin Grabnar P (2020) Excipients in freeze-dried biopharmaceuticals: contributions toward formulation stability and lyophilisation cycle optimisation. Int J Pharm 576:1

95. Mohan HK, Livieratos L, Peters AM (2019) Lung clearance of inhaled aerosol of Tc-99m-methoxyisobutyl isonitrile: relationships with cigarette smoking, age and gender. Clin Physiol Funct Imaging 39:236–239. https://doi.org/10.1111/cpf.12562

96. Galindo-Filho VC, Ramos ME, Rattes CSF et al (2015) Radio-aerosol pulmonary deposition using mesh and jet nebulizers during noninvasive ventilation in healthy subjects. Respir Care 60:1238–1246. https://doi.org/10.4187/respcare.03667

97. Galindo-Filho VC, Alcoforado L, Rattes C et al (2019) A mesh nebulizer is more effective than jet nebulizer to nebulize bronchodilators during non-invasive ventilation of subjects with COPD: a

randomized controlled trial with radiolabeled aerosols. Respir Med 153:60–67. https://doi.org/10.1016/j.rmed.2019.05.016

98. Kuehl PJ, Chand R, McDonald JD et al (2019) Pulmonary and regional deposition of nebulized and dry powder aerosols in ferrets. AAPS PharmSciTech. https://doi.org/10.1208/s12249-019-1382-3

99. LaFrance N, Fournier F (2020) Radioaerosols and the updated EANM guideline in ventilation/perfusion imaging. Eur J Nucl Med Mol Imaging 47:1640–1642

100. Paiva DN, Masiero PR, Spiro BL et al (2012) Continuous positive airway pressure and body position alter lung clearance of the radiopharmaceutical 99mtechnetium-diethylenetriaminepentaacetic acid (99mTc-DTPA). Afr J Biotechnol 11:16519–16524. https://doi.org/10.5897/ajb12.2563

101. Dugernier J, Reychler G, Wittebole X et al (2016) Aerosol delivery with two ventilation modes during mechanical ventilation: a randomized study. Ann Intens Care. https://doi.org/10.1186/s13613-016-0169-x

102. de Albuquerque IM, Cardoso DM, Masiero PR et al (2016) Effects of positive expiratory pressure on pulmonary clearance of aerosolized technetium-99m-labeled diethylenetriaminepentaacetic acid in healthy individuals. J Bras Pneumol 42:404–408. https://doi.org/10.1590/s1806-37562015000000320

103. Reychler G, Aubriot AS, Depoortere V et al (2014) Effect of drug targeting nebulization on lung deposition: a randomized crossover scintigraphic comparison between central and peripheral delivery. Respir Care 59:1501–1507. https://doi.org/10.4187/respcare.03068

104. Mesquita FOS, Galindo-Filho VC, Neto JLF et al (2014) Scintigraphic assessment of radio-aerosol pulmonary deposition with the acapella positive expiratory pressure device and various nebulizer configurations. Respir Care 59:328–333. https://doi.org/10.4187/respcare.02291

105. Galindo-Filho VC, Brandão DC, de Ferreira RCS et al (2013) Noninvasive ventilation coupled with nebulization during asthma crises: a randomized controlled trial. Respir Care 58:241–249. https://doi.org/10.4187/respcare.01371

106. Karacavus S, Intepe YS (2015) The role of Tc-99m DTPA aerosol scintigraphy in the differential diagnosis of COPD and asthma. Clin Respir J 9:189–195. https://doi.org/10.1111/crj.12123

107. Lang O, Balon HR, Pichova R et al (2013) Lung tissue density measured by low-dose CT during pulmonary perfusion SPECT/CT as a tool for differentiation pulmonary embolism from chronic obstructive pulmonary disease—a pilot study. Cor Vasa. https://doi.org/10.1016/j.crvasa.2013.10.002

108. Dixon DL, de Pasquale CG, Lawrence MD et al (2017) Lung fluid clearance in chronic heart failure patients. Int J Cardiol 244:245–247. https://doi.org/10.1016/j.ijcard.2017.05.096

109. Ono CR, Tedde ML, Scordamaglio PR, Buchpiguel CA (2018) Pulmonary inhalation-perfusion scintigraphy in the evaluation of bronchoscopic treatment of bronchopleural fistula. Radiol Bras 51:385–390. https://doi.org/10.1590/0100-3984.2017.0133

110. Chortarea S, Fytianos K, Rodriguez-Lorenzo L et al (2018) Distribution of polymer-coated gold nanoparticles in a 3D lung model and indication of apoptosis after repeated exposure. Nanomedicine 13:1169–1185. https://doi.org/10.2217/nnm-2017-0358

111. Wang H, Sebrié C, Ruaud JP et al (2016) Aerosol deposition in the lungs of spontaneously breathing rats using Gd-DOTA-based contrast agents and ultra-short echo time MRI at 1.5 Tesla. Magn Reson Med 75:594–605. https://doi.org/10.1002/mrm.25617

112. Bianchi A, Gobbo OL, Dufort S et al (2017) Orotracheal manganese-enhanced MRI (MEMRI): an effective approach for lung tumor detection. NMR Biomed. https://doi.org/10.1002/nbm.3790

113. Graczyk H, Bryan LC, Lewinski N et al (2015) Physicochemical characterization of nebulized superparamagnetic iron oxide nanoparticles (SPIONs). J Aerosol Med Pulm Drug Deliv 28:43–51. https://doi.org/10.1089/jamp.2013.1117

114. Price DN, Kunda NK, Muttil P (2019) Challenges associated with the pulmonary delivery of therapeutic dry powders for preclinical testing. KONA Powder Part J 36:129–144. https://doi.org/10.14356/kona.2019008

115. Ivey JW, Vehring R, Finlay WH (2015) Understanding pressurized metered dose inhaler performance. Expert Opin Drug Deliv 12:901–916. https://doi.org/10.1517/17425247.2015.984683

116. Nord A, Linner R, Milesi I et al (2020) A novel delivery system for supraglottic atomization allows increased lung deposition rates of pulmonary surfactant in newborn piglets. Pediatr Res 87:1019–1024. https://doi.org/10.1038/s41390-019-0696-x

117. Evbuomwan O, Purbhoo K, Vangu MDT (2018) A prospective study comparing 99m Tc-MIBI and 99m Tc-MDP with 99m Tc-DTPA for lung ventilation scintigraphy in pulmonary thromboembolism. Nucl Med Commun 39:1103–1112. https://doi.org/10.1097/MNM.0000000000000913

118. Bennett WD, Zeman KL, Laube BL et al (2018) Homogeneity of aerosol deposition and mucociliary clearance are improved following ivacaftor treatment in cystic fibrosis. J Aerosol Med Pulm Drug Deliv 31:204–211. https://doi.org/10.1089/jamp.2017.1388

119. Rathor VPS, Chugh P, Ali R et al (2016) Formulation, preclinical and clinical evaluation of a new submicronic arginine respiratory fluid for treatment of chronic obstructive pulmonary disorder. Saudi Pharmaceut J 24:49–56. https://doi.org/10.1016/j.jsps.2015.03.010

120. Mohan HK, Routledge T, Cane P et al (2016) Does the clearance of inhaled 99mTc-sestamibi correlate with multidrug resistance protein 1 expression in the human lung? Radiology 280:924–930. https://doi.org/10.1148/radiol.16151389

121. Sá RC, Zeman KL, Bennett WD et al (2015) Effect of posture on regional deposition of coarse particles in the healthy human lung. J Aerosol Med Pulm Drug Deliv 28:423–431. https://doi.org/10.1089/jamp.2014.1189

122. van Aswegen H, van Aswegen A, du Raan H et al (2013) Airflow distribution with manual hyperinflation as assessed through gamma camera imaging: a crossover randomised trial. Physiotherapy (UK) 99:107–112. https://doi.org/10.1016/j.physio.2012.05.007

123. Ditcham W, Murdzoska J, Zhang G et al (2014) Lung deposition of 99mTc-radiolabeled albuterol delivered through a pressurized metered dose inhaler and spacer with facemask or mouthpiece in children with asthma. J Aerosol Med Pulm Drug Deliv. https://doi.org/10.1089/jamp.2014.1139

124. Usmani OS, Baldi S, Warren S et al (2022) Lung deposition of inhaled extrafine beclomethasone dipropionate/formoterol fumarate/glycopyrronium bromide in healthy volunteers and asthma: the STORM study. J Aerosol Med Pulm Drug Deliv. https://doi.org/10.1089/jamp.2021.0046

125. Taylor G, Warren S, Dwivedi S et al (2018) Gamma scintigraphic pulmonary deposition study of glycopyrronium/formoterol metered dose inhaler formulated using co-suspension delivery technology. Eur J Pharm Sci 111:450–457. https://doi.org/10.1016/j.ejps.2017.10.026

126. Leach CL, Kuehl PJ, Chand R, McDonald JD (2016) Respiratory tract deposition of HFA-beclomethasone and HFA-fluticasone in asthmatic patients. J Aerosol Med Pulm Drug Deliv 29:127–133. https://doi.org/10.1089/jamp.2014.1199